Maturilli *et al. Earth, Planets and Space* (2016) 68:84
DOI 10.1186/s40623-016-0464-7

Earth, Planets and Space

LETTER

Open Access

On the effect of emergence angle on emissivity spectra: application to small bodies

Alessandro Maturilli*, Jörn Helbert, Sabrina Ferrari and Mario D'Amore

Abstract

Dependence of laboratory-measured emissivity spectra from the emergence angle is a subject that still needs a lot of investigations to be fully understood. Most of the previous work is based on reflectance measurements in the VIS–NIR spectral region and on emissivity measurements of flat, solid surfaces (mainly metals), which are not directly applicable to the analysis of remote sensing data. Small bodies in particular (c.f. asteroids Itokawa and 1999JU3, the respective targets of JAXA Hayabusa and Hayabusa 2 missions) have a very irregular surface; hence, the spectra from those rough surfaces are difficult to compare with laboratory spectra, where the observing geometry is always close to "nadir." At the Planetary Emissivity Laboratory of the German Aerospace Center (DLR), we have set up a series of spectral measurements to investigate this problem in the 1- to 16-μm spectral region. We measured the emissivity for two asteroid analogue materials (meteorite Millbillillie and a synthetic enstatite) in vacuum and under purged air, at surface temperature of 100 °C, for emergence angles of 0°, 5°, 10°, 20°, 30°, 40°, 50°, and 60°. Emissivity of a serpentinite slab, already used as calibration target for the MARA instrument on Hayabusa 2 MASCOT lander and for the thermal infrared imager spectrometer on Hayabusa 2 orbiter, was measured under the same conditions. Additionally, a second basalt slab was measured. Both slabs were not measured at 5° inclination. Complementary reflectance measurements of the four samples were taken. For all the samples measured, we found that for calibrated emissivity, significant variations from values obtained at nadir (0° emergence angle) appear only for emergence angles ≥40°. Reflectance measurements confirmed this finding, showing the same trend of variations.

Keywords: The Hayabusa 2 mission, Asteroid analogue materials, Emissivity measurements, Emergence angle, Infrared spectroscopy

Introduction

The photometric features of planetary surface simulants have been already studied from several authors. Gunderson et al. (2006, 2007) observed the photometric properties for visible (VIS) and near-infrared (NIR) reflectance measurements of Martian regolith simulants. Shepard and Helfenstein (2007) tested the Hapke photometric model with a goniometer in the 0.4- to 0.9-μm spectral range. Hapke (himself) et al. (2009) tested its theoretical model on bidirectional reflectance with the help of goniometric measurements in the visible spectral range. Again a goniometer study in the VIS spectral range was carried out from Shepard and Helfenstein (2013) to study the bidirectional reflectance spectra from particulate samples. Beck et al. (2012) measured the bidirectional reflectance phase function of several meteorite samples in the VIS spectral range. Pommerol et al. (2013) measured the bidirectional reflectance of Martian analogues in dry, wet, and frozen conditions over a wide range of phase angles in the visible spectral range. Visible/near-infrared reflectance measurements of lunar soil simulants, Apollo soils, and Martian analogue samples as functions of illumination and emission angles were described in Johnson et al. (2013).

The influence of emergence (or observing) angle (θ) on the measured emissivity of natural surfaces has already

*Correspondence: alessandro.maturilli@dlr.de
German Aerospace Center DLR, Institute of Planetary Research, Rutherfordstr. 2, 12489 Berlin, Germany

been observed. Labed and Stoll (1991) studied the angular variation of the thermal infrared emissivity of natural samples under laboratory conditions. They observed that a decrease of the emissivity with increasing viewing angle does exist, and it is not simply related to the optical properties of the material, but it depends also on the scattering mechanism, grain size, porosity, etc. However, the setup they used for the experiment was very rudimentary, so they could only measure samples in air and had to restrict their spectral range to three segments: 3.2–4.2, 4.4–5.5, and 8.0–13.5 μm. In their conclusions, they state that the emissivity decreases with increasing viewing angle. For sand and silty material in small pieces, the effect is very weak up to $\theta = 60°$. A very simplified experiment on water and ice showed the same kind of angular dependence for emissivity in the thermal infrared (8–14 μm) region (Rees and James 1992). Wald and Salisbury (1995) measured in air thermal infrared (7–14 μm) directional emissivity of quartz for several particle size ranges and packing fractions. Emissivity was found to be a strong function of each of these variables. In particular, for small grain sizes (where thermal gradients in the samples are higher), the angular dependence is non-monotonic, with a peak at $\theta = 45°$. A successive study conducted to provide angular emissivity measurements for five representative samples (water, clay, sand, loam, and gravel) in one thermal IR broadband (8–13 μm) showed a general decrease in emissivity with increasing viewing angles (Cuenca and Sobrino 2004). The authors acknowledged that for all the samples, there is no significant difference in measured emissivity for θ from 0° to 30°. Finally, a recent study on the angular variation of thermal infrared (7.7–14.3 μm) emissivity (ε) for twelve inorganic bare soil (IBS) types concluded that ε of all IBS studied is almost azimuthally isotropic, and also zenithally up to $\theta = 40°$, from which ε values decrease significantly with the increase of θ (García-Santos et al. 2012).

Building on these coherent indications from previous literature, we decided in this work to focus on the experimental verification of the effect of increasing emergence angle on emissivity measurements for asteroid analogue materials, taking into high consideration the results from the Hayabusa mission (Okada et al. 2015). We therefore selected a fine particle sample of meteorite Millbillillie, an achondritic eucrite originating from asteroid Vesta (Hiroi et al. 1995; McSween et al. 2013; Mittelfehldt 2014), and a synthetic enstatite to represent E-type asteroids (Zellner et al. 1977), both reduced to <25 μm as analogues for asteroid surface. The selection of those two samples does not explore the vast collection of asteroid analogues. Nevertheless, our intent in this study is to show that deviation of directional emissivity from ideal case has a trend that is independent from the kind of target sample we chose for the measurements; also our choice of two powdered samples plus two slab samples is reasonable from a statistical point of view.

We measured their emissivity under purging air and vacuum (<0.8 mbar) conditions, at 100 °C surface temperature, using the setup described in Helbert et al. (2013) and adjusted for measuring at lower temperature, for emergence angles from 0° to 60°. The choice of measuring at 100 °C surface temperature is not fully representative for NEOs, but it was a set point high enough to have good signal for measuring emissivity and low enough to remain a realistic approximation for the daily surface temperature of many asteroids.

Reflectance spectra were measured (for samples at room temperature, a standard condition in this kind of measurements) with minimal incidence angle ($i = 13°$) and emergence angles ranging from 13° to 80° (see Maturilli et al. 2014). A solid serpentinite sample, used for the calibration of MARA instrument on MASCOT lander and for the thermal infrared imager instrument of the Hayabusa 2 mission (Helbert et al. 2014), was measured in emissivity and reflectance under the same conditions. A second basalt slab was used to confirm the results found by measuring the serpentinite slab sample. Even if igneous rocks like basalts are not to be found on asteroids, this sample contained large phenocrysts of olivine and pyroxenes, commonly considered as asteroid analogue materials (Gaffey et al. 1993). This second slab was measured not because of its nature of asteroid analogue material, but as a thin slab sample, whose measurements were easier, trustworthy, and useful to confirm our findings on the other asteroid analogues we measured in this work. Furthermore, the surface of asteroids is composed of fine particle as well as larger particles. It is impossible to measure coarse particles in our setup, because the larger grains tend to slip away, even for small emergence angles. For this reason, the slab measurements are really important to support the results we found for finer particles, because the slabs offer the possibility to have reliable measurements on a target with physical features close to those of large grain size particles.

Methods

At PEL, we use two instruments equipped with external chambers to measure emissivity. The Bruker Vertex 80 V Fourier transform infrared (FTIR) spectrometer is operated under vacuum to remove atmospheric features from the spectra. An external evacuable chamber is used to measure emissivity: It contains a motor-driven carousel for up to 12 samples in the same working session, thermal sensors for each sample, and a webcam for monitoring the activities inside the chamber. The induction heating system allows heating up the samples (in stainless steel

cups) from 50 °C to higher than 800 °C (Helbert et al. 2013). A Bruker A513 accessory mounted in the same spectrometer is used to obtain bi-conical reflectance with variable incidence angle i and emission angle e between 13° and 85° at room temperature, under purged (dry air, H_2O, and CO_2 removed) or vacuum conditions, in the 1- to 100-μm spectral range (Maturilli et al. 2014). In the whole spectral range, a gold sandpaper-coated surface is used as reference for reflectance measurements, measured with the same incidence and emission angles as the samples. The incidence beam cone angle is of 17°, the incidence beam size depends on the incidence angle, and it is however smaller than 10 mm, being the sample cup/reference diameter size for reflectance measurements.

The air-purged Bruker IFS 88 FTIR spectrometer has an attached emissivity chamber for measurements at low to moderate temperatures (Maturilli et al. 2006, 2008) that can be cooled down to 0 °C. Samples can be heated from room temperature to 150 °C in a purging environment. A Harrick Seagull™ variable-angle reflection accessory allows measurement of the bi-conical reflectance at room temperature, under purging conditions in the extended spectral range from 0.4 to 55 μm, for i and e from 5° to 85°.

In this work, emissivity in vacuum was measured with the Bruker Vertex 80 V, emissivity under purged air with the Bruker IFS 88. The two instruments have similar optical design, but some design differences cause the field of view (FOV) of the Vertex 80 V to be double in size to the one for the IFS 88 instrument. Emissivity was always measured using sample cups having 50 mm diameter. For emissivity measurements at 5° and 10°, emergence angle aluminum wedges were used, while for all the emergence angles from 20° to 60° (in 10° steps) we used custom-designed stainless steel wedges (see Fig. 1). Powdered meteorite Millbillillie, synthetic enstatite (grain sizes <25 μm), and a serpentinite slab were chosen as analogues for asteroid surface. Furthermore, a second basalt slab was used to confirm our results.

To avoid slipping, the powdered samples were packed by mixing them with ethanol and then dried in oven at 350 K. Ethanol allows particles to rearrange and homogeneously distribute. As ethanol evaporates, the particles network results compressed into a denser packing, increasing the frictional resistance to sliding. Desiccation treatment in an oven removes residual capillary bridges. Since ethanol is not effective as solvent on the minerals of both samples, no solid bridges occurrence is expected during the evaporation (Gohering et al. 2013). For each sample a temperature sensor was carefully placed in contact with the emitting layer to ensure a sample surface temperature of 100 °C. Each sample was calibrated in emissivity with respect to a blackbody measured at exactly the same temperature and for emergence angle 0° to reproduce the calibration procedure of an instrument onboard a spacecraft orbiting around an asteroid. A waiting time of 1 h was observed before each measurement to stabilize the sample temperature.

Bi-conical reflectance measurements were taken in vacuum with an A513 accessory unit, setting incidence angle to the minimum possible ($i = 13°$) and varying the emission angle between 13° and 80°. In a recent paper, we show that bi-conical reflectance spectra of samples measured at PEL under purging or under vacuum conditions are identical (Maturilli et al. 2015).

Emissivity and reflectance measurements with both instruments were achieved by using a nitrogen-cooled MCT detector coupled with a KBr beam splitter. For emissivity and reflectance measurements, 4 cm^{-1} was used as spectral resolution.

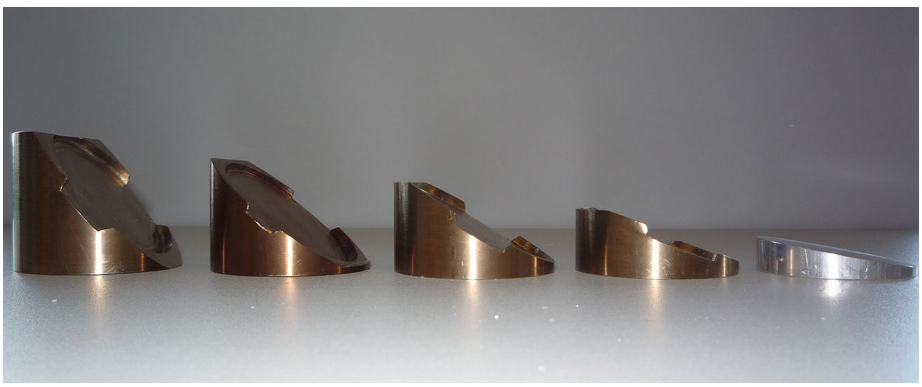

Fig. 1 Wedges for inclined emissivity measurements; for 5° and 10° emergence angles aluminum wedges were manufactured, while for 20°–60° emergence angle, custom-designed and custom-made stainless steel wedges were used to heat up the samples at the proper emission angle

Results and discussion

The study presented in this manuscript is designed to investigate the influence of increasing emergence angle on the emissivity measurements of asteroid's analogue materials. Figure 2 shows emissivity spectra measured under purged air for a powdered Millbillillie sample for emergence angle from 0° to 60°. Each spectrum was calibrated with respect to a "flat" or "nadir" ($\theta = 0°$) blackbody measured at the same temperature as the sample. 1−R (R is bi-conical reflectance at minima i and e angles) is shown for mere comparison too. For $\theta < 40°$, the spectral variations are very limited, and from $\theta = 40°$, we can observe that the emissivity spectra of the inclined surfaces tend to diverge from the one measured in nadir geometry. The band peaking at the Christiansen feature (CF, a maximum in emissivity, see Maturilli et al. 2006) around 8.1 μm is narrowing with increasing θ, while the whole continuum tends to lower. To numerically quantify the effect of increasing emergence angle on measured emissivity, we calculated the average percent difference between emissivity with $\theta = 0°$ and all the other values for θ. For each point in the 5- to 14-μm spectral range, the absolute value of $(\varepsilon_\theta - \varepsilon_{\theta=0})$ was divided for $\varepsilon_{\theta=0}$ to express the difference in percent. The average value (expressed in %) of those differences along all the point in the 5- to 14-μm spectral range is used as average error between ε_θ and $\varepsilon_{\theta=0}$.

In the paper of Maturilli and Helbert (2014), the maximum error on a single emissivity measurement along the whole continuum at PEL was studied and found to be $\sigma = 0.35$ %. We decided to apply those results to our current work, proposing that the divergence from emissivity measured in nadir geometry can be considered significant when exceeding the value of $2\sigma = 0.7$ %. Table 1 shows those results for emissivity difference of Millbillillie measured under purged air.

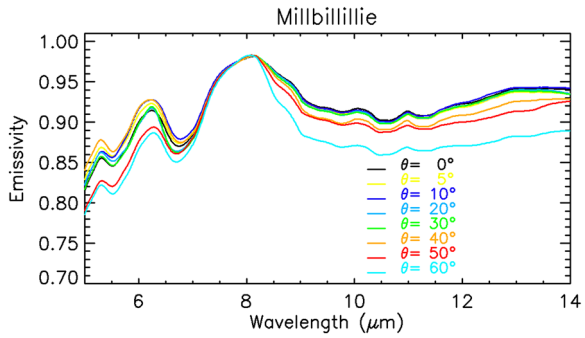

Fig. 2 Millbillillie emissivity measured under purged air for increasing θ; emissivity spectra of meteorite Millbillillie <25 μm sample measured under purged air at 100 °C surface temperature, for increasing emergence angle (θ), calibrated with respect to a blackbody at the same surface temperature, measured under nadir viewing geometry

Table 1 Percent deviation from nadir ($\theta = 0°$) for emissivity of Millbillillie measured under purging environment

Emissivity difference (%) at variable θ for Millbillillie under purged atmosphere	
$\theta = 5°$	0.46 %
$\theta = 10°$	0.48 %
$\theta = 20°$	0.39 %
$\theta = 30°$	0.34 %
$\theta = 40°$	1.35 %
$\theta = 50°$	1.86 %
$\theta = 60°$	3.45 %

Table 1 highlights that emissivity variations become significant for $\theta \geq 40°$.

Figure 3 shows the same kind of measurements for a synthetic enstatite sample. Again, the spectra show that emissivity deviation from "nadir"-like measurements occurs around $\theta = 40°$. We can detect the same narrowing of the band peaking at the CF and lowering of the continuum like for the Millbillillie sample. Deviations originating from increasing values of θ for the synthetic enstatite sample are reported in Table 2. Emissivity variations become again relevant for $\theta \geq 40°$, in agreement with deviations observed for the Millbillillie sample under the same conditions.

Similar emissivity measurements have been performed on two slabs, except for the measurements at 5° emergence angle, which was omitted because they would be redundant for this study. The first sample is a serpentinite slab, already used as a calibration body for the instrument MARA on MASCOT lander and the thermal infrared imager on the JAXA Hayabusa 2 mission (Helbert et al. 2014). The slab is much thicker than the usual samples used in the PEL laboratory (20 mm with respect to 3–5 mm as usual sample thicknesses). The resulting change in the measurement geometry could potentially affect the measured emissivity, because the FOV of the measurements could include the side portion of the slab. Figure 4 shows the serpentinite slab emissivity dependence on the increasing emergence angle θ. In this case too it can be noted that starting from $\theta = 40°$ the emissivity spectra show larger divergence from a nadir measurement. The relative deviations of emissivity from $\theta = 0°$ for increasing angle θ are listed in Table 3. We believe that the high value of emissivity deviation occurring for $\theta = 20°$ is a measurement error, probably caused from a not perfect position of the sample (because of its geometrical dimension) under the mirror collecting the emitted radiation to the spectrometer.

Nevertheless, despite the different height of this slab sample making the measurements trickier, the emissivity variations become significant for $\theta \geq 40°$.

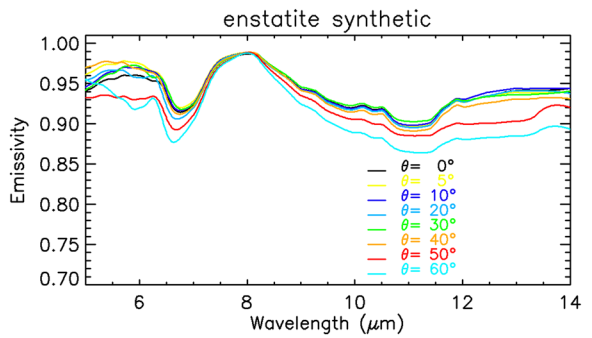

Fig. 3 Synthetic enstatite emissivity measured under purged air for increasing θ; emissivity spectra of synthetic enstatite <25 μm sample measured under purged air at 100 °C surface temperature, for increasing emergence angle (θ), calibrated with respect to a blackbody at the same surface temperature, measured under nadir viewing geometry

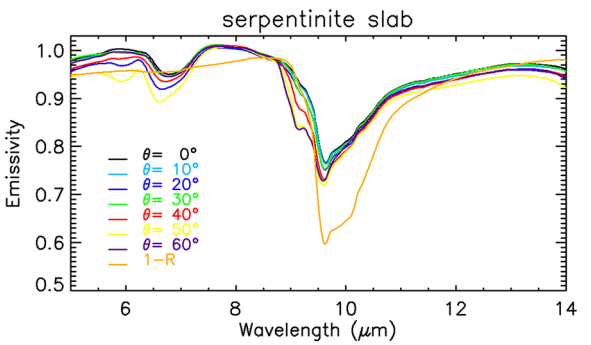

Fig. 4 Serpentinite slab emissivity measured under purged air for increasing θ; emissivity spectra of serpentinite slab sample measured under purged air at 100 °C surface temperature, for increasing emergence angle (θ), calibrated with respect to a blackbody at the same surface temperature, measured under nadir viewing geometry. 1−R (R = bi-conical reflectance) is shown for comparison too

Table 2 Percent deviation from nadir ($\theta = 0°$) for emissivity of synthetic enstatite measured under purging environment

Emissivity difference (%) at variable θ for synthetic enstatite under purged atmosphere	
$\theta = 5°$	0.37 %
$\theta = 10°$	0.41 %
$\theta = 20°$	0.45 %
$\theta = 30°$	0.45 %
$\theta = 40°$	0.89 %
$\theta = 50°$	1.79 %
$\theta = 60°$	2.65 %

Table 3 Percent deviation from nadir ($\theta = 0°$) for emissivity of serpentinite slab measured under purging environment

Emissivity difference (%) at variable θ for serpentinite slab under purged atmosphere	
$\theta = 10°$	0.41 %
$\theta = 20°$	1.80 %
$\theta = 30°$	0.42 %
$\theta = 40°$	1.55 %
$\theta = 50°$	3.56 %
$\theta = 60°$	1.18 %

To avoid the effects caused by the excessive height of this slab on the measured emissivity (cf. excessive deviation for $\theta = 20°$), we repeated the measurements on a basalt slab with a thickness of 5 mm, closer to the standards used at PEL. While we do not consider the basalt itself as an analogue for asteroid surfaces, the measured sample provides several phenocrysts of olivine and pyroxenes, whose solid-solution phases are commonly identified as possible asteroid surface components. Figure 5 shows the results of emissivity measurements for this material, while Table 4 lists the emissivity differences with respect to nadir geometry data.

For the two powdered samples, we measured emissivity for increasing θ under vacuum ($P < 0.8$ mbar), at surface temperature of 100 °C. Figure 6 shows the spectra we measured for a Millbillillie sample. Again, we detect the narrowing of the band peaking at the CF and lowering of the continuum like for the measurements under purged air. We do not perform a direct comparison between emissivity and reflectance in vacuum because of the complications originating from the effect of thermal gradients (see Salisbury et al. 1994) on emissivity measurements of powdered samples in vacuum. Typical effects of thermal gradients on the measured emissivity spectra of powdered samples are band shifting, loss of spectral contrast, and band narrowing. However, in this paper we are only comparing measurements taken under the same conditions, and as our results show, the deviation of directional emissivity from the ideal case is not depending on the atmospheric pressure used for the experiment.

Table 5 confirms the trend we already observed for purged measurements, showing that emissivity variations become significant for $\theta \geq 40°$. High emissivity deviation for $\theta = 20°$ is probably originating from a not precise positioning of the sample on the wedge under the parabolic mirror.

Figure 7, picturing the same results for a synthetic enstatite under vacuum, shows that for $\theta \geq 50°$ measured emissivity undergoes a first important step in its changing.

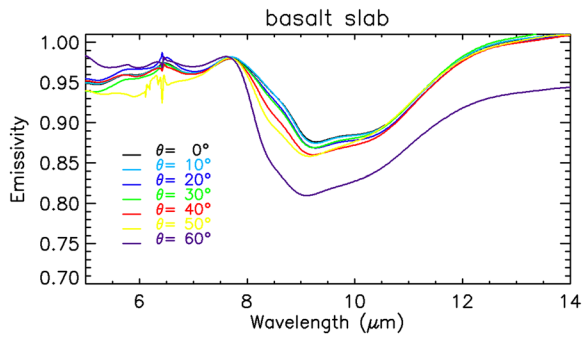

Fig. 5 Basalt slab emissivity measured under purged air for increasing θ; emissivity spectra of basalt slab sample measured under purged air at 100 °C surface temperature, for increasing emergence angle (θ), calibrated with respect to a blackbody at the same surface temperature, measured under nadir viewing geometry

Table 4 Percent deviation from nadir ($\theta = 0°$) for emissivity of basalt slab measured under purging environment

Emissivity difference (%) at variable θ for basalt slab under purged atmosphere	
$\theta = 10°$	0.07 %
$\theta = 20°$	0.49 %
$\theta = 30°$	0.49 %
$\theta = 40°$	0.64 %
$\theta = 50°$	1.40 %
$\theta = 60°$	3.63 %

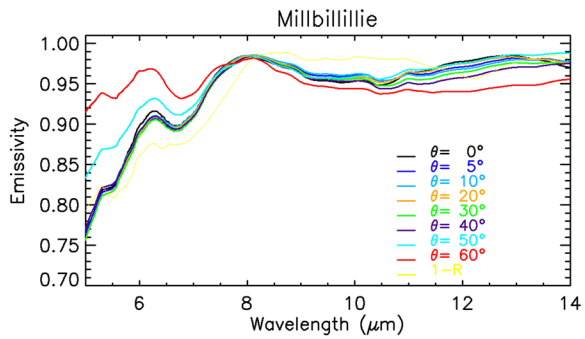

Fig. 6 Millbillillie emissivity measured under vacuum for increasing θ; emissivity spectra of meteorite Millbillillie <25 μm sample measured under vacuum at 100 °C surface temperature, for increasing emergence angle (θ), calibrated with respect to a blackbody at the same surface temperature, measured under nadir viewing geometry. 1−R (R = bi-conical reflectance) is shown for comparison too

Table 6 confirms the trend we already observed for purged measurements, with emissivity variations again becoming significant for $\theta \geq 40°$. Small deviations from this general behavior (like the apparent maximum at $\theta = 30°$) are due to difficulties in optimizing the geometrical/optical setup for the measurements. In fact, our instrument field of view for measurements under vacuum doubles the one for measurements under purging. Therefore, tilting the sample when increasing the emergence angle results in diminishing the amount of sample surface exposed to the mirror collecting the emitted radiation, hence increasing the portion of cup and wedge (made of

Table 5 Percent deviation from nadir ($\theta = 0°$) for emissivity of Millbillillie measured under vacuum

Emissivity difference (%) at variable θ for Millbillillie under vacuum	
$\theta = 5°$	0.48 %
$\theta = 10°$	0.36 %
$\theta = 20°$	0.99 %
$\theta = 30°$	0.13 %
$\theta = 40°$	1.25 %
$\theta = 50°$	6.17 %
$\theta = 60°$	6.15 %

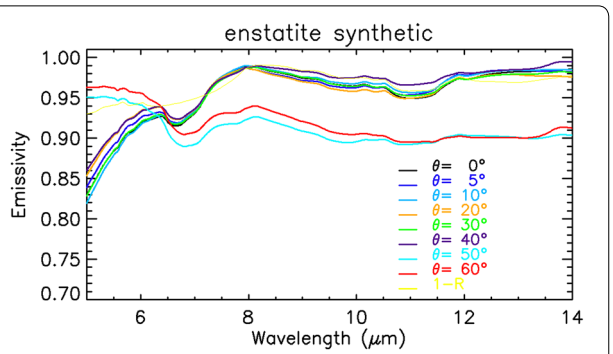

Fig. 7 Synthetic enstatite emissivity measured under vacuum for increasing θ; emissivity spectra of synthetic enstatite <25 μm sample measured under vacuum at 100 °C surface temperature, for increasing emergence angle (θ), calibrated with respect to a blackbody at the same surface temperature, measured under nadir viewing geometry. 1−R (R = bi-conical reflectance) is shown for comparison too

Table 6 Percent deviation from nadir ($\theta = 0°$) for emissivity of synthetic enstatite measured under vacuum

Emissivity difference (%) at variable θ for synthetic enstatite under vacuum	
$\theta = 5°$	0.49 %
$\theta = 10°$	0.46 %
$\theta = 20°$	0.46 %
$\theta = 30°$	0.70 %
$\theta = 40°$	0.59 %
$\theta = 50°$	2.01 %
$\theta = 60°$	5.28 %

steel) radiation included in the measurements, and since the emissivity of steel is much lower than for the sample, this explains the high variations that we see in Figs. 6 and 7 for measured emissivity at values of $\theta \geq 50°$.

We measured bi-conical reflectance of the same samples, reproducing the optical/geometrical conditions we posed for the emissivity experiment. We put the incident angle to the minimum (the Sun in nadir position with respect to the surface) and moved the emission angle from the minimum (13°) to 20° and then to 80°, step 10°. Figure 8 shows the measurements (we show 1−R, R = reflectance, for a direct comparison with emissivity) for Millbillillie, and Fig. 9 shows the reflectance measured for synthetic enstatite.

Table 7 (differences in % for Millbillillie, calculated with respect to R taken for $\theta = 13°$) and Table 8 (differences in % for synthetic enstatite, calculated with respect to R taken for $\theta = 13°$) help us to understand the trend for those measurements. As we did for emissivity spectra, we compare those differences with the 2σ error we characterized in Maturilli et al. (2014). It is interesting to note that for Millbillillie, different and independent measurement methods like emissivity and reflectance produce the same result as can be seen from Table 5 and Table 7: The first detectable deviation from nadir-like measurements is occurring for angles above $\theta = 30°$. Further analysis will be conducted to understand if this effect has a physical explanation.

The reflectance measurements confirm what we already found with emissivity measurements: For $\theta \geq 40°$ "nadir"-like measurements could be misleading to approximate the spectra we got from a surface with high inclination (hence emergence angle) θ.

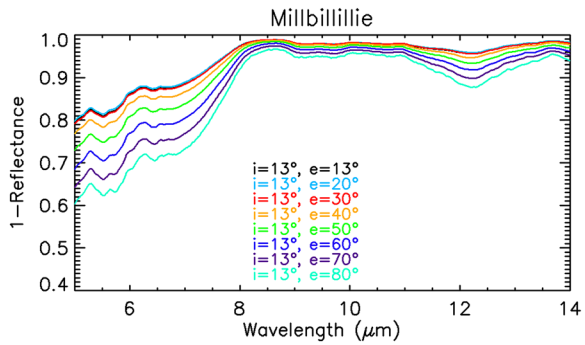

Fig. 8 Millbillillie 1-reflectance measured under vacuum for increasing emergence angle (*e*); 1-reflectance spectra of meteorite Millbillillie <25 μm sample measured under vacuum at room temperature, for fixed (minimum) incidence angle ($i = 13°$) and increasing emergence angle (*e*), calibrated with respect to a gold sandpaper reference, measured under the same incidence and emission angles

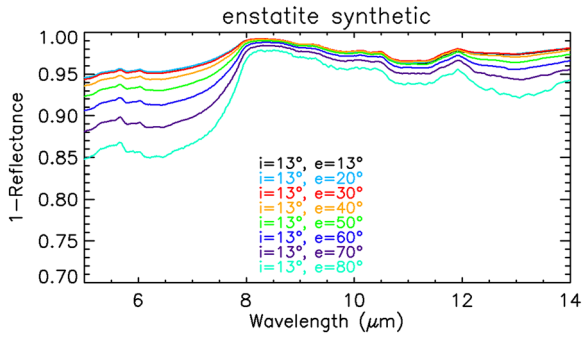

Fig. 9 Synthetic enstatite 1-reflectance measured under vacuum for increasing emergence angle (*e*); 1-reflectance spectra of synthetic enstatite <25 μm sample measured under vacuum at room temperature, for fixed (minimum) incidence angle ($i = 13°$) and increasing emergence angle (*e*), calibrated with respect to a gold sandpaper reference, measured under the same incidence and emission angles

Table 7 Percent deviation from nadir ($\theta = 13°$) for 1−R of Millbillillie measured under vacuum

1−R difference (%) at variable θ for Millbillillie under vacuum	
$\theta = 20°$	0.26 %
$\theta = 30°$	0.01 %
$\theta = 40°$	1.59 %
$\theta = 50°$	3.87 %
$\theta = 60°$	6.67 %
$\theta = 70°$	9.66 %
$\theta = 80°$	12.57 %

Table 8 Percent deviation from quasi-nadir ($\theta = 13°$) for 1−R of synthetic enstatite measured under vacuum

1−R difference (%) at variable θ for synthetic enstatite under vacuum	
$\theta = 20°$	0.04 %
$\theta = 30°$	0.19 %
$\theta = 40°$	0.72 %
$\theta = 50°$	1.77 %
$\theta = 60°$	3.28 %
$\theta = 70°$	5.61 %
$\theta = 80°$	8.82 %

Conclusions

To test the influence of increasing emergence angle on measured emissivity and reflectance spectra of small bodies (especially for asteroids), we set up a suite of experiments at the Planetary Emissivity Laboratory (PEL) of the German Aerospace Center (DLR). Two powdered analogue materials, meteorite Millbillillie and synthetic enstatite, were measured in emissivity at 100 °C surface

temperature, under vacuum and purged air conditions, for emergence angles from 0° to 60°. A serpentinite slab and a basalt slab were measured under the same conditions. Reflectance measurements on powders were taken for minimum incidence angle ($i = 13°$) and emergence angle (e) varying from 13° to 80°. All the spectra were measured between 5 and 14 μm.

For all the target samples we found that divergence from nadir-like measurement becomes significant for emergence angles $\theta \geq 40°$.

Our results have a direct application for different fields of study. For planetary surfaces (where for gravitational effects, the surface slopes and therefore emergence angles are typically low), the effect of emergence angles can be largely neglected. On small bodies, however, large surface slopes and regions of highly irregular surface topographies are observed due to the microgravity environment. The resulting high emergence angles can lead to a misinterpretation of the spectral data if compared to laboratory measurements of analogues measured under nadir viewing geometries. Thermophysical models of small bodies (cf. Davidsson et al. 2015) should take into account our results for regions of high emergence angles ($\theta \geq 40°$).

Analyses on our emissivity and reflectance measurements show that emergence angles $\theta < 40°$ do not affect the spectra significantly, while for $\theta \geq 40°$ we detect significant spectral differences, further increasing for each 10° step of increasing emergence angle θ. Similar results are obtained by a goniometric study on variations of emitted energy depending on the emergence angle carried out with the Oxford Space Environment Goniometer (OSEG) of the Oxford University (Warren et al. 2015).

Abbreviations

JAXA: Japan Aerospace Exploration Agency; PEL: Planetary Emissivity Laboratory; DLR: Deutsche Zentrum für Luft- und Raumfahrt e. V (German Aerospace Agency); MARA: MAscot RAdiometer; MASCOT: Mobile Asteroid Surface Scout; TIR: thermal infrared imager; IR: infrared; IBS: inorganic bare soils; OSEG: Oxford Space Environment Goniometer; FTIR: Fourier transform infrared; MCT: mercury cadmium telluride; CF: Christiansen feature; FOV: field of view.

Authors' contributions

AM designed the study, including all the setup modifications and adaptations, and performed all the measurements. JH participated to the design of the study and to the data analysis. SF contributed to the measuring process and to data calibration and analysis. MD'A helped with the discussion of the results and with drafting the manuscript. All authors read and approved the final manuscript.

Authors' information

AM is a postdoc at the Institute of Planetary Research of the German Aerospace Center (DLR) in Berlin, Germany. He is co-investigator in several ESA planetary mission and part of the scientific team in NASA and JAXA missions. He is the laboratory manager of the Planetary Emissivity Laboratory (PEL). JH is leader of the Planetary Spectroscopy Laboratory group at the Institute of Planetary Research of the German Aerospace Center (DLR) in Berlin, Germany. He is Co-PI of the MERTIS instrument on BepiColombo and CoI of several instruments, among them are the TIR and MARA instruments on Hayabusa 2. SF is a postdoc at the Institute of Planetary Research of the German Aerospace Center (DLR) in Berlin, Germany. MD'A is a postdoc at the Institute of Planetary Research of the German Aerospace Center (DLR) in Berlin, Germany.

Acknowledgements

All the authors are founded by the German Aerospace Center (DLR). The Planetary Emissivity Laboratory (PEL) is founded and operated by the German Aerospace Center (DLR).

Competing interests

The authors declare that they have no competing interests.

Received: 30 April 2015 Accepted: 6 May 2016
Published online: 23 May 2016

References

Beck P, Pommerol A, Thomas N, Schmitt B, Moynier F, Barrat JA (2012) Photometry of meteorites. Icarus 218:364–377

Cuenca J, Sobrino JA (2004) Experimental measurements for studying angular and spectral variation of thermal infrared emissivity. Appl Opt 43(23):4598–4602

Davidsson BJR, Rickman H, Bandfield JL, Groussin O, Gutiérrez PJ, Wilska M, Capria MT, Emery JP, Helbert J, Jorda L, Maturilli A, Mueller TG (2015) Interpretation of thermal emission. I. The effect of roughness for spatially resolved atmosphereless bodies. Icarus 252:1–21

Gaffey MJ, Bell JF, Hamilton Brown R, Burbine TH, Piatek JL, Reed KL, Chaky DA (1993) Mineralogical variations within the S-type asteroid class. Icarus 106:573–602

García-Santos V, Valor E, Caselles V, Ángeles Burgos M, Coll C (2012) On the angular variation of thermal infrared emissivity of inorganic soils. J Geophys Res. doi:10.1029/2012JD017931

Gohering L, Nakahara A, Dutta T, Kitsunezaki S, Tarafdar S (2013) Desiccation cracks and their patterns: formation and modelling in science and nature. Wiley, New York

Gunderson K, Thomas N, Whitby JA (2006) First measurements with the Physikalisches Institut Radiometric Experiment (PHIRE). Planet Space Sci 54:1046–1056

Gunderson K, Lüthi B, Russell P, Thomas N (2007) Visible/NIR photometric signatures of liquid water in Martian regolith simulant. Planet Space Sci 55:1272–1282

Hapke BW, Shepard MK, Nelson RM, Smythe WD, Piatek JL (2009) A quantitative test of the ability of models based on the equation of radiative transfer to predict the bidirectional reflectance of a well-characterized medium. Icarus 199:210–218

Helbert J, Maturilli A, D'Amore M (2013) Visible and near-infrared reflectance spectra of thermally processed synthetic sulfides as a potential analog for the hollow forming materials on Mercury. EPSL 369–370:233–238. doi:10.1016/j.epsl.2013.03.045

Helbert J, Del Togno S, Maturilli A, Ferrari S, Grott M, Borgs B, Okada T (2014) A novel spectral and radiometric calibration target for the TIR imager and the MARA instrument on the Hayabusa2 mission. In: 45th lunar and planetary science conference 2014. The Woodlands, Texas, 17–21 Mar 2014, Abstract 1317

Hiroi T, Binzel RP, Sunshine JM, Pieters CM, Takeda H (1995) Grain sizes and mineral compositions of surface regoliths of vesta-like asteroids. Icarus 115:374–386

Johnson JR, Shepard MK, Grundy WM, Paige DA, Foote EJ (2013) Spectrogoniometry and modeling of Martian and lunar analog samples and Apollo soils. Icarus 223:383–406

Labed J, Stoll MP (1991) Angular variation of land surface spectral emissivity in the thermal infrared: laboratory investigations on bare soils. Int J Remote Sens 12(11):2299–2310. doi:10.1080/01431169108955259

Maturilli A, Helbert J (2014) Characterization, testing, calibration, and validation of the Berlin emissivity database. J Appl Remote Sens. doi:10.1117/1.JRS.8.084985

Maturilli A, Helbert J, Witzke A, Moroz L (2006) Emissivity measurements of analogue materials for the interpretation of data from PFS on Mars Express and MERTIS on Bepi-Colombo. PSS 54(11):1057–1064

Maturilli A, Helbert J, Moroz L (2008) The Berlin emissivity database (BED). PSS 56(3–4):420–425
Maturilli A, Helbert J, StJohn JM, Head JW III, Vaughan WM, D'Amore M, Gottschalk M, Ferrari S (2014) Komatiites as Mercury surface analogues: spectral measurements at PEL. EPSL 398:58–65. doi:10.1016/j.epsl.2014.04.035
Maturilli A, Helbert J, D'Amore M, Ferrari S (2015). Experimental verification of validity for Kirchhoff's law (E = 1-R) in vacuum and purged air. In: 46th lunar and planetary science conference 2015. The Woodlands, Texas, 16–20 Mar 2015, Abstract 1722
McSween HY Jr, Binzel RP, De Sanctis MC, Ammannito E, Prettyman TH, Beck AW, Reddy V, Le Corre L, Gaffey MJ, McCord TB, Raymond CA, Russell CT, the Dawn Science Team (2013) Dawn; the Vesta–HED connection; and the geologic context for eucrites, diogenites, and howardites. Meteorit Planet Sci 48(11):2090–2104
Mittlefehldt DW (2014) Asteroid (4) Vesta: I. The howardite-eucrite-diogenite (HED) clan of meteorites. Chemie der Erde Geochem 75(2):155–183
Okada T, Zolensky ME, Ireland TR, Yada T (2015) The *Earth, Planets and Space* Special Issue: "Science of solar system materials examined from Hayabusa and future missions". Earth Planets Space 67:1–4. doi:10.1186/s40623-015-0235-x
Pommerol A, Thomas N, Jost B, Beck P, Okubo C, McEwen AS (2013) Photometric properties of Mars soils analogs. JGR 118:2045–2072. doi:10.1002/jgre.20158
Rees WG, James SP (1992) Angular variation of the infrared emissivity of ice and water surfaces. Int J Remote Sens 13(15):2873–2886. doi:10.1080/01431169208904088
Salisbury JW, Wald A, D'Aria DM (1994) Thermal-infrared remote sensing and Kirchhoff's law 1. Laboratory measurements. JGR 99(B6):11897–11911
Shepard MK, Helfenstein P (2007) A test of the Hapke photometric model. JGR 112:E03001. doi:10.1029/2005JE002625
Shepard MK, Helfenstein P (2013) A laboratory study of the bidirectional reflectance from particulate samples. Icarus 215:526–533
Wald AE, Salisbury JW (1995) Thermal infrared directional emissivity of powdered quartz. J Geophys Res 100(B12):24665–24675
Warren T, Arnold J, Thomas I, Lindsay S, Greenhagen B, Bowles N (2015) Investigating surface roughness effects on the directional emissivity of surfaces using the oxford space environment goniometer. In: 46th lunar and planetary science conference 2015. The Woodlands, Texas, 16–20 Mar 2015, Abstract 1744
Zellner B, Leake M, Morrison D, Williams JG (1977) The E asteroids and the origin of the enstatite achondrites. Geochim Cosmochim Acta 41(12):1759–1767